Soft Matter

Modes of Adhesion of Two Janus Nanoparticles on the Outer or Inner Side of Lipid Vesicles

Journal:	*Soft Matter*
Manuscript ID	SM-ART-03-2022-000306.R1
Article Type:	Paper
Date Submitted by the Author:	05-May-2022
Complete List of Authors:	Zhu, Yu; The University of Memphis, Physics and Materials Science Sharma, Abash; The University of Memphis, Physics and Material Science Spangler, Eric; The University of Memphis, Physics and Materials Science Laradji, Mohamed; The University of Memphis, Physics and Materials Science

Modes of Adhesion of Two Janus Nanoparticles on the Outer or Inner Side of Lipid Vesicles

Yu Zhu, Abash Sharma, Eric J. Spangler, and Mohamed Laradji*
Department of Physics and Materials Science, The University of Memphis, Memphis, TN 38152, USA

Using molecular dynamics simulations of a coarse-grained model, in conjunction with the weighted histogram analysis method, the adhesion modes of two spherical Janus nanoparticles (NPs) on either the outer or inner side of lipid vesicles are explored. In particular, the effects of the area fraction, J, of the NPs that interacts attractively with the lipid head groups, the adhesion strength and the size of the NPs on their adhesion mode are investigated. The NPs are found to exhibit two main modes of adhesion when adhered to the outer side of the vesicle. In the first mode, which occurs at relatively low values of J, the NPs are apart from each other. In the second mode, which occurs at higher values of J, the NPs form an in-plane dimer. Janus NPs, which adhere to the inner side of the vesicle, are found to always be apart from each other, regardless of the value of J and their diameter.

I. INTRODUCTION

The understanding of the interaction between nanoparticles (NPs) and lipid membranes is important to the development of effective and safe nanomaterials for a wide range of biomedical applications and, potentially, for harnessing lipid membranes as an alternative tool for bottom-up fabrication of ordered nanostructures [1]. Attractive forces between certain water-soluble NPs and a lipid membrane lead to the adhesion of the NPs on the membrane while causing its deformations which extend over length-scales beyond the size of the NPs [2–5]. In turn, these deformations induce effective interactions between the NPs, which can result in their self-assembly on the membrane [1, 6–17]. Many computational studies have been conducted, during recent years, to investigate membrane-induced interactions between spherical NPs [13, 16], cap-shaped NPs [18], and anisotropic NPs [19–21] including highly anisotropic crescent-shaped NPs [14, 22–26].

Janus NPs form a special class of nanomaterials which are designed to have two moieties with different chemical compositions [27–30]. Several studies have been conducted to understand the interaction between Janus NPs with lipid membranes [18, 31–35]. For example, it was shown through both simulations and experiments that amphiphilic Janus NPs, with one hydrophilic moiety and one hydrophobic moiety, induce rupture of lipid membranes [34, 35]. Janus spherical NPs, with one moiety that interacts attractively with the lipid head groups and the other moiety that is hydrophilic but interacts repulsively with the lipid membrane, are particularly interesting since while they tend to adhere to lipid membranes, they are not as disruptive as amphiphilic Janus NPs. The maximum amount of wrapping of such hydrophilic Janus NPs, by lipid membranes, is limited by the area fraction, J, of the moiety that interacts attractively with the lipid membrane. This is contrasted with uniform spherical NPs whose degree of wrapping depends on the strength of the adhesion energy density and the size of the NPs [15].

Using molecular dynamics simulations of an implicit-solvent model, Reynwar *et al.* [18] showed earlier that the adhesion of small, almost spherical Janus NPs, with diameter about the thickness of the bilayer, lead to large deformations of the membrane, and form small clusters which are eventually endocytosed. More recently, Bahrami and Weikl [31] showed, through a Monte Carlo energy minimization of dynamically triangulated vesicles, that the preferred placement of Janus NPs on vesicles depends on J and whether the NPs adhere to the inner or outer side of the vesicle. They found that when the NPs adhere to the outer side of the vesicle, they prefer to be apart from each other for small and moderate values of J. However, for relatively large values of J, the NPs dimerize. In contrast, they found that the NPs are always apart from each other, when they adhere to the inner side of the vesicle, regardless of the value of J. In this approach, which does not account for thermal fluctuations, the contribution of the NPs' adhesion potential energy to the total energy is interestingly found to be independent of the distance between the NPs. As a result, the minimization of the total energy reduces to the minimization of the membrane curvature energy. Furthermore, the membrane topology is conserved in this approach. Therefore, endocytosis or exocytosis of the NPs, which may happen at high degrees of wrapping, are not accounted for in [31].

The goal of the present investigation is to further elucidate the adhesion of spherical Janus NPs on lipid vesicles through a realistic approach which accounts for thermal fluctuations and topological changes of the membrane. This is achieved through a systematic set of simulations based on molecular dynamics of a coarse-grained implicit-solvent model with varying values of the adhesion energy density, size of the NPs and fraction of the NPs area that interact attractively with the lipids. In this approach, a NP is modeled as a hollow sphere whose surface is con-

*Email: mlaradji@memphis.edu

structed as a triangular mesh obtained from successive tessellations of a regular icosahedron [36], and the vertices of the mesh are occupied by beads. To provide rigidity to the NP, its beads are connected by harmonic springs and three-body interactions. The NP's rigidity is further enhanced by inserting a bead at its center and by connecting it to all surface beads with fairly rigid harmonic springs. In order to unambiguously determine the equilibrium state of the system, the free energy is determined using the weighted histogram analysis method [37] with the distance between the NPs as its reaction coordinate. Both cases of NPs adhering to the outer and inner sides of the vesicle were investigated over values of J ranging between 0.1 and 0.9.

The article is organized as follows. In Section II, the model and computational approach are presented. The results are then presented and discussed in Section III. Here, results are presented for the case of Janus NPs adhering to the outer and inner sides of the vesicle. Finally, a summary and conclusion of this work are found in Section IV.

II. MODEL AND COMPUTATIONAL METHOD

The present study uses an implicit-solvent model of self-assembled lipid membranes [38, 39], in which a lipid molecule is coarse-grained into a short semi-flexible chain composed of one head (h) bead and two tail (t) beads. Essential ingredients of the model are presented below. Further details are found in Appendix A of Ref. [16]. The potential energy of the lipid bilayer is given by

$$U\left(\{\mathbf{r}_i\}\right) = \sum_{i,j} U_0^{\alpha_i\alpha_j}\left(r_{ij}\right) + \sum_{\langle i,j\rangle} U_{\text{bond}}^{\alpha_i\alpha_j}\left(r_{ij}\right) + \sum_{\langle i,j,k\rangle} U_{\text{bend}}^{\alpha_i\alpha_j\alpha_k}\left(\mathbf{r}_i,\mathbf{r}_j,\mathbf{r}_k\right), \quad (1)$$

where $\mathbf{r}_i$ denotes the coordinates of bead i, $r_{ij}=|\mathbf{r}_i-\mathbf{r}_j|$, and $\alpha_i(=h \text{ or } t)$ denotes the type of bead i. The angular bracket in the second summation of Eq. (1) indicates that i and j are bonded within the same lipid chain. Likewise, the angular bracket in the third summation indicates that i, j and k are part of the same lipid chain. In Eq. (1), $U_0^{\alpha\beta}$ is a soft two-body potential, between beads of types α and β. This interaction is given by Eq. (A2) in Appendix A of Ref. [16]. Due to the absence of explicit solvent in this model, the self-assembly of the lipid chains into bilayers is achieved through a short-range attractive interaction between the t beads. Otherwise, h-h and h-t interactions are repulsive [39].

In Eq. (1), $U_{\text{bond}}^{\alpha_i\alpha_j}$ ensures connectivity between beads that belong to the same lipid chain and is given by

$$U_{\text{bond}}^{\alpha_i\alpha_j}(r_{ij}) = \frac{k_{\text{bond}}^{\alpha_i\alpha_j}}{2}\left(r_{ij}-a_{\alpha_i\alpha_j}\right)^2, \quad (2)$$

where $k_{\text{bond}}^{\alpha_i\alpha_j}$ is the bond stiffness coefficient and $a_{\alpha_i\alpha_j}$ is the preferred bond length between beads i and j of types α_i and α_j, respectively. It is noted that in addition to this bonding interaction, in this model, bonded beads within a lipid chain also interact with each other through $U_0^{\alpha_i\alpha_j}$.

Finally, in Eq. (1), $U_{\text{bend}}^{\alpha\beta\gamma}$ is a three-body potential that provides bending stiffness to the lipid chains and is given by

$$U_{\text{bend}}^{\alpha_i\alpha_j\alpha_k}\left(\mathbf{r}_i,\mathbf{r}_j,\mathbf{r}_k\right) = \frac{k_{\text{bend}}^{\alpha_i\alpha_j\alpha_k}}{2}\left(\cos\varphi_0 - \frac{\mathbf{r}_{ij}\cdot\mathbf{r}_{kj}}{r_{ij}r_{kj}}\right)^2, \quad (3)$$

where k_{bend} is the bending stiffness coefficient and φ_0 is the preferred splay angle of the lipid chain, taken to be 180°. The bending rigidity of the membrane can be modified by tuning the strength of the hydrophobic interaction, U_0^{tt}, and the strength of the three body interaction, k_{bend}^{htt} [39].

A Janus NP is initially constructed as an icosahedron mesh followed by three subsequent tessellations, resulting into 642 nodes (beads of type n) and 1280 elementary triangles [36]. The nodes are then projected onto a sphere, of diameter D_{np}, with same center as the original icosahedron. Two neighboring beads of the NP are connected via the harmonic potential given by Eq. (2) with a bond stiffness k_{bond}^{nn} and a preferred bond length $a_{nn}=l$. To provide further rigidity to the NP, the three body interaction, given by Eq. (3) with a bending stiffness coefficient k_{bend}^{nnn}, is added to every connected triplet of beads. The preferred splay angle φ_0^{nnn} of each triplet is determined from the initial configuration of the NP.

Since a NP is hollow in this model, the two-body and three-body interactions are found not to be sufficient to provide a very rigid spherical structure, unless k_{bond}^{nn} and k_{bend}^{nnn} are very high, which is not desirable since this would require very small values of the integration time step. This problem is circumvented by inserting a bead of type c, at the center of the NP, which is bonded to all surface n-beads by a harmonic potential given by Eq. (2) with a bond stiffness k_{bond}^{cn} and a preferred bond length $a_{cn}=D_{np}$.

A Janus NP is comprised of two types of beads, corresponding to n_a and n_b beads. The interaction between the NP beads with the lipid beads is also given by Eq. (A2) in Appendix A of Ref. [16]. Both n_a and n_b beads are hydrophilic, i.e. they interact repulsively with the lipid tail beads ($U_{\text{min}}^{n_at}=U_{\text{min}}^{n_bt}=0$). To promote the adhesion of the n_a beads on the membrane, the interaction between the n_a beads with the lipid head beads is attractive, i.e. $U_{\text{min}}^{n_ah}=\mathcal{E}<0$. The Janus nature of the NP is ensured by making the interaction between the n_b and the lipid head beads repulsive, i.e. $U_{\text{min}}^{n_bh}=0$. Beads belonging to different NPs interact with each via the same two-body potential $U_0^{\alpha_i\alpha_j}$. This interaction is chosen to be fully repulsive ($U_{\text{min}}^{n_an_a}=U_{\text{min}}^{n_bn_b}=U_{\text{min}}^{n_an_b}=0$) to prevent NPs from aggregation in the absence of lipid membranes. The term Janusity (J) is introduced to define the area fraction of the NP that interacts attractively with the lipid head groups, i.e. $J=d/D_{np}$, where d is

the height of the spherical cap that interacts attractively with the lipid head beads, as indicated by Fig. 1 for the case of $J = 0.5$. We note that the parameters of the NP model can be tuned to affect the rigidity and the roughness of the NPs surface.

All beads are moved using a molecular dynamics scheme with a Langevin thermostat [40],

$$\dot{\mathbf{r}}_i(t) = \mathbf{v}_i(t) \quad (4)$$

$$m\dot{\mathbf{v}}_i(t) = -\nabla_i U(\{\mathbf{r}_i\}) - \Gamma \mathbf{v}_i(t) + \sigma \boldsymbol{\Xi}_i(t), \quad (5)$$

where m is the mass of a bead (same for all beads), Γ is a bead's friction coefficient, and $\sigma\boldsymbol{\Xi}_i(t)$ is a random force originating from the heat bath. $\boldsymbol{\Xi}_i(t)$ is a random vector generated from a uniform distribution and obeys $\langle \boldsymbol{\Xi}_i(t) \rangle = 0$ and $\langle \Xi_i^{(\mu)}(t)\, \Xi_j^{(\nu)}(t') \rangle = \delta_{\mu\nu}\delta_{ij}\delta(t-t')$, where μ and $\nu = x$, y or z. The dissipative and random forces are interrelated through the dissipation-fluctuation theorem, which leads to $\Gamma = \sigma^2/2k_{\mathrm{B}}T$.

The model interaction parameters used in the simulations are,

$$\begin{aligned}
U_{\mathrm{max}}^{hh} &= U_{\mathrm{max}}^{ht} = 100\epsilon, \\
U_{\mathrm{max}}^{tt} &= 200\epsilon, \\
U_{\mathrm{min}}^{hh} &= U_{\mathrm{min}}^{ht} = 0, \\
U_{\mathrm{min}}^{tt} &= -6\epsilon, \\
U_{\mathrm{max}}^{n_a h} &= 200\epsilon, \\
U_{\mathrm{min}}^{n_a h} &= -\mathcal{E}, \\
U_{\mathrm{max}}^{n_b h} &= U_{\mathrm{max}}^{n_b t} = u_{\mathrm{max}}^{n_a t} = 100\epsilon, \\
U_{\mathrm{min}}^{n_b h} &= u_{\mathrm{min}}^{n_b t} = u_{\mathrm{min}}^{n_a t} = 0, \\
U_{\mathrm{max}}^{n_a n_a} &= U_{\mathrm{max}}^{n_a n_b} = U_{\mathrm{max}}^{n_b n_b} = 200\epsilon, \\
U_{\mathrm{min}}^{n_a n_a} &= U_{\mathrm{min}}^{n_a n_b} = U_{\mathrm{min}}^{n_b n_b} = 0, \\
k_{\mathrm{bond}}^{ht} &= k_{\mathrm{bond}}^{tt} = 100\epsilon/r_m^2, \\
k_{\mathrm{bend}}^{htt} &= 100\epsilon, \\
k_{\mathrm{bond}}^{nn} &= 1200\epsilon, \\
k_{\mathrm{bond}}^{nc} &= 45\epsilon/r_m^2, \\
k_{\mathrm{bend}}^{nnn} &= 250\epsilon, \\
r_c &= 2r_m, \\
a_{ht} &= a_{tt} = 0.7r_m, \\
a_{cn} &= D_{np}. \quad (6)
\end{aligned}$$

The simulations are performed on vesicles composed of $N = 50\,000$ lipids. This corresponds to a vesicle diameter $D_{ves} = 76$ nm. Here, D_{ves} is defined as twice the average distance between the positions of the h-beads of the outer leaflet and the vesicle's center of mass. The results in this article are shown for two NP diameters corresponding to $D_{np} = 10$ and 20 nm. All simulations are executed at $k_BT = 3.0\epsilon$, with a time step $\Delta t = 0.02\tau$ for $D_{np} = 20$ nm and $\Delta t = 0.015\tau$ for $D_{np} = 10$ nm, where $\tau = r_m(m/\epsilon)^{1/2}$. Eqs. (4) and (5) are integrated using the velocity-Verlet algorithm [41] with $\Gamma = \sqrt{6}m/\tau$. The vesicle is placed in three-dimensional boxes, with periodic boundary conditions along the x-, y- and z-axes, with a linear size equal to $2D_{ves}$. This ensures that interaction between the vesicle and itself through the periodic boundary conditions does not occur.

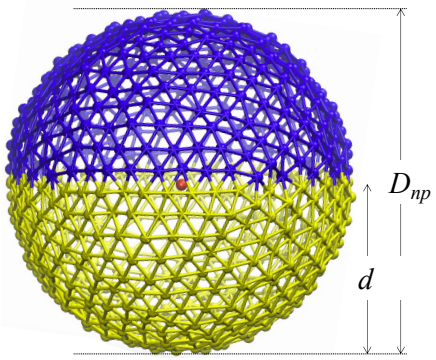

FIG. 1: Configuration of a spherical Janus NP at time $t = 50\tau$ with $D_{np} = 20$ nm. Only yellow beads are able to adhere to the lipid membrane, the red bead is locates at the center of NP, and is connected to all other beads by harmonic bonds (not shown for clarity) to maintain a spherical shape of the NP. In this case, the Janusity $J = d/D_{np} = 0.5$. Here, d is the height of the spherical cap that interacts attractively with the lipid head beads.

The bending modulus of the bare membrane, with the interaction parameters given by Eq. (6), and as extracted from the spectrum of the height fluctuations of a tensionless bilayer, is $\kappa \approx 30k_BT$ [39], which is comparable to the bending modulus of a DPPC bilayer in the fluid phase [42]. From comparison of the thickness of the present model bilayer in the fluid phase, which is very close to $4r_m$, with that of a typical fluid phospholipid bilayer (≈ 4 nm), the small length scale $r_m \approx 1$ nm. Hence, in the remainder of this article, all lengths are expressed in nanometers and energies are expressed in k_BT.

To determine the adhesion energy density of the NPs on the membrane, simulations of a uniform NP (i.e., a Janus NP with $J = 1$) on a tensionless planar membrane are performed at different values of $\mathcal{E}$ (which corresponds to the minimum of the potential energy between a n_a bead and an h bead). The adhesion energy density is then defined as $\xi = |E_{adh}|/A_{adh}$, where E_{adh} is the net potential energy between the NP and the membrane and A_{adh} is the area of the NP adhering to the membrane. Here, an n_a bead adheres to the membrane if it interacts with at least one h bead of the membrane, i.e. if its distance from the h bead is less than r_c. The dependence of the adhesion energy density ξ on $\mathcal{E}$ is depicted in Fig. 2 for the cases of $D_{np} = 10$ and 20 nm. This figure shows that for low values of $\mathcal{E}$, ξ's dependence on $\mathcal{E}$ is not linear. However, this dependence becomes linear for $\mathcal{E} \gtrsim \epsilon$. Since the number of beads per NP is 642 regardless of its diameter, the adhesion energy density, for a given $\mathcal{E}$ decreases with increasing D_{np}.

The degree of wrapping of a NP by the lipid membrane

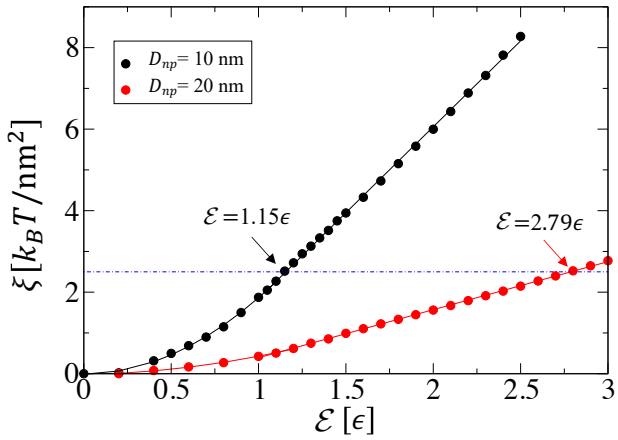

FIG. 2: The adhesion energy density, ξ, versus the absolute value of the interaction strength, $\mathcal{E}$, between a NP a-bead and a lipid head bead. Black and red symbols correspond to $D_{np} = 10$ and 20 nm, respectively. The solid lines are fits of the data. The blue line indicates that an arbitrary energy density $\xi = 2.5 k_BT/\mathrm{nm}^2$ corresponds to $\mathcal{E} = 1.15\epsilon$ for $D_{np} = 10$ nm and $\mathcal{E} = 2.79\epsilon$ for $D_{np} = 20$ nm. The increased value of $\mathcal{E}$ with D_{np}, for a given value of energy density ξ, is due to the fact that both 10-nm and 20-nm NPs are composed of same number of beads.

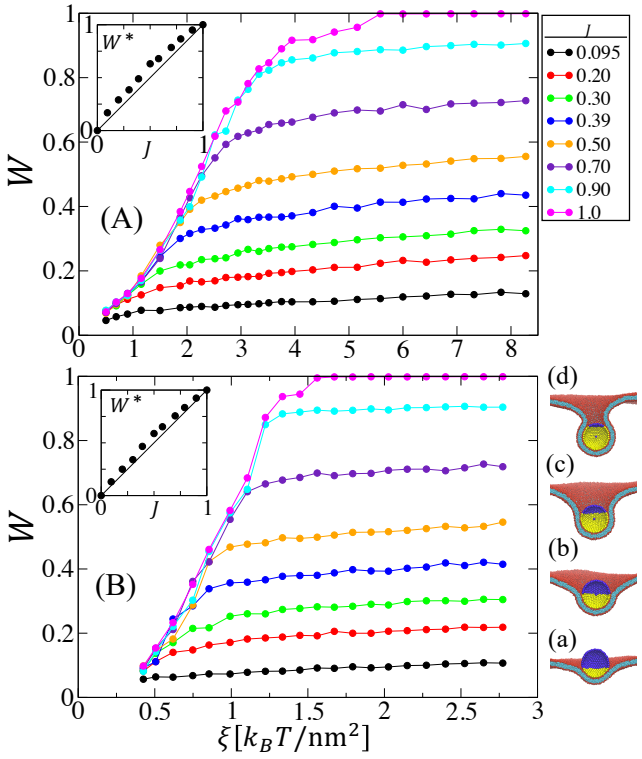

FIG. 3: Degree of wrapping W, defined by Eq. (7), versus ξ for different values of the Janusity J obtained from a simulation of a single 10-nm and 20-nm Janus NP on a planar lipid bilayer. (A) and (B) correspond to $D_{np} = 10$ and 20 nm, respectively. The insets show the extrapolated value of W as $\xi \to \infty$ as a function of J. The solid line in the inset corresponds to $y = x$. Snapshots (a), (b), (c), and (d) correspond to $J = 0.3$. 0.5, 0.7, and 0.9, respectively, for the case of $D_{np} = 20$ nm at $\xi = 1.56\ k_BT/\mathrm{nm}^2$. Only a fraction of the membrane, around the NP, is shown in these snapshots.

is defined by the following quantity,

$$W = \frac{1}{2}(1 - \cos\theta), \tag{7}$$

where the wrapping angle $\theta \in [0, \pi]$, is calculated as follows: For each azimuthal angle $\varphi \in [0, 2\pi)$, around the z-axis, a latitude angle $\theta_{\max}(\varphi)$ is determined as the maximum latitude angle of lipid head beads within 1.3 nm from the NP's surface. The wrapping angle θ is then defined as the average of $\theta_{\max}$ over φ. W is extracted numerically in the case of NPs adhering to a tensionless planar bilayer. Figs. 3(A) and (B) show that regardless of the NP's size, the dependence of the degree of wrapping on ξ follows two main regimes. For small values of ξ, W is lower than J and increases rapidly with ξ. For large values of ξ, the increase of W with J is much slower and asymptotically saturates to a value W^* that increases with increasing J. The crossover between the two regimes is due to the repulsive interaction between the n_b and h beads, which limits the degree of wrapping. The insets of both Figs. 3(A) and (B) show that W^*, which is obtained from the extrapolation of W to $\xi \to \infty$ (through plotting W versus $1/\xi$, then taking the limit $1/\xi \to 0$), is almost equal to J, with W slightly larger than J for mid values of J.

Fig. 3 also shows that the value of ξ at which the dependence of W on ξ crosses from the rapid increase to the saturation regime decreases with increasing D_{np}. For example, in the case of $J = 0.7$, the crossover is at $\xi \approx 3$ and 1 k_BT/nm^2 for $D_{np} = 10$ and 20 nm, respectively. This is due to the fact that a maximum amount of wrapping for a particular value of J occurs when the curvature energy, which is about $8\kappa JA/D_{np}^2$ is about the adhesion energy ξJA, where $A = \pi D_{np}^2$, i.e when $\xi D_{np}^2 \approx 8\kappa$ [3]. Therefore, the adhesion energy density at saturation $\xi^* \sim 1/D_{np}^2$. This agrees well with Fig. 3, which shows that the ratio $\xi^*_{10\mathrm{nm}}/\xi^*_{20\mathrm{nm}} \approx 3.7$, which is close to 4.

To determine the equilibrium state of the vesicle with two adhering Janus NPs, a series of umbrella sampling simulations were performed with a reaction coordinate corresponding to the distance d between the centers of mass of the NPs [43]. The following bias harmonic potential energy between the center beads of the two NPs is used

$$U_{bias}(d) = \frac{k_{bias}}{2}(d - d_{bias})^2, \tag{8}$$

where k_{bias} is varied between 10ϵ and 20ϵ, and the preferred distance d_{bias} is varied between $D_{np} + \lambda$ and

$D_{np} + D_{ves}$, where λ is slightly smaller than r_m. The step in r_{bias} is chosen to be sufficiently small so that there is an appreciable amount of overlap between consecutive histograms of the distance between the NPs generated from the biased simulations. The weighted histogram analysis method (WHAM) [37] was then used to obtain the unbiased free energy of the vesicle with two NPs as a function of the distance d.

III. RESULTS

A. Adhesion of Two Janus NPs on the Outer Leaflet of a Vesicle

Figs. 4 (A) and (B) show the distance between the NPs as a function of time for the cases of $J = 0.30$ and 0.58, respectively, with an initial distance between the NPs, $d(0) = 11$ and 60 nm. Fig. 4 (A) demonstrates that for $J = 0.30$, the NPs prefer to be apart from each other, regardless of their initial placement on the vesicle. In contrast, at $J = 0.58$, the final state of the NPs depends on their initial placement on the vesicle. When the initial distance between them is relatively large, the NPs tend to remain apart from each other in a monomeric state, as demonstrated by Fig. 4 (B). However, Fig. 4 (B) shows that the distance between the NPs remain small, if the initial placement between the NPs is small, i.e. the NPs are dimerized in this case. This figure therefore implies that at the higher value of J, there exist an energy barrier

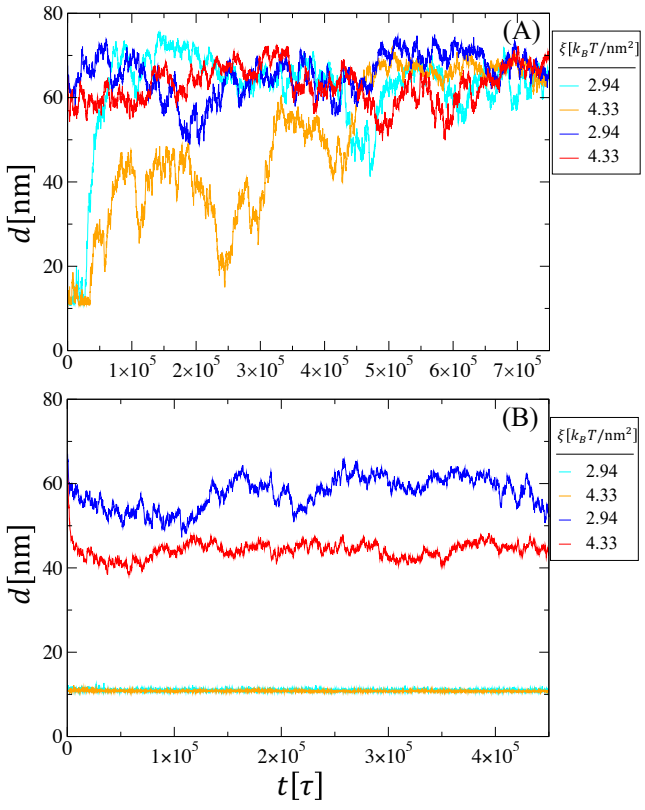

FIG. 4: Distance between 10-nm NPs, adhering to the outer side of a vesicle, versus time for the case of $J = 0.30$ (A) and $J = 0.58$ (B). Blue and red curves correspond to the case where the initial distance between the NPs is 60 nm. Cyan and orange curves correspond to the case where the initial distance between the NPs is 11 nm. The values of the adhesion energy density are indicated in the legends.

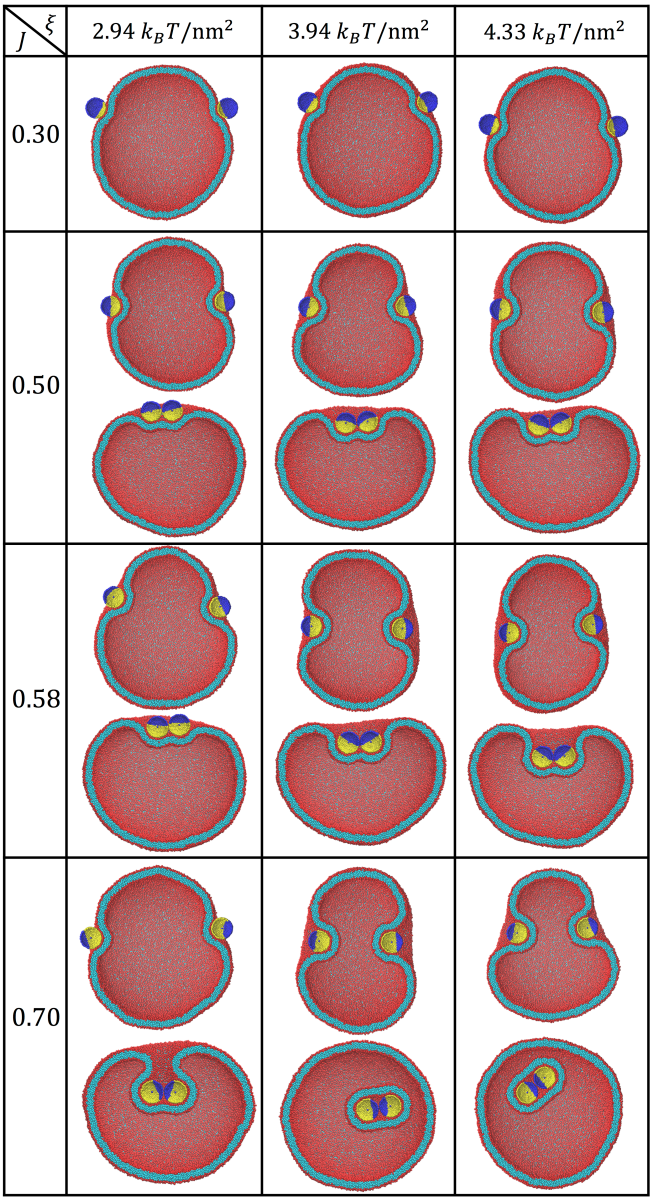

FIG. 5: Preferred configurations of 10-nm NPs, adhering to the outer side of a vesicle, with different values of J and at different values of the adhesion energy density ξ. Lipid head and tail beads are red and cyan, respectively. NP beads that interact attractively with the lipid head beads are yellow. NP beads that interact repulsively with both head and tail lipid beads are blue. The center beads of the NPs are colored blue

between the monomeric and dimeric state that is much higher than the thermal energy. It is noted that for low values of the Janusity, the NPs are weakly wrapped by the membrane, as indicated by Fig. 3. As a result, NPs with low J are highly diffusive on the vesicle, regardless of the adhesion strength.

Typical equilibrium configurations at different values of J and adhesion strength are shown in Fig. 5. This figure shows, again, that at low values of J, *e.g.* $J = 0.30$, the NPs prefer to be apart from each other. However at higher values of J, the final state depends on the initial separation between the NPs as discussed earlier. Fig. 5 demonstrates qualitatively that the amount of wrapping experienced by the NPs increases with increasing either Janusity or adhesion energy density. This figure also shows that when the two NPs are dimerized, they are localized in a pit which turns into a bud with a narrow neck as J or ξ is increased (e.g. see lower snapshots at $(J, \xi) = (0.58, 4.33 k_B T/\text{nm}^2)$ and $(0.70, 2.94 k_B T/\text{nm}^2)$ in Fig. 5. For high values of J and values of ξ, the dimerized NPs are endocytosed in a single vesicle, as shown by the upper snapshots at $(J, \xi) = (0.70, 3.94 k_B T/\text{nm}^2)$ or $(0.70, 4.33 k_B T/\text{nm}^2)$ in Fig. 5. In contrast, the NPs in the monomeric state are not endocytosed even at high values of J ($J \lesssim 0.8$) and ξ, as shown by Fig. 3, in contrast to the case of uniform spherical NPs which of course can be endocytosed by vesicles and planar membranes [5, 44, 45]. Therefore, the endocytosis of the Janus NPs with $J < 1$ is facilitated by their dimerization. This is due to the fact that as the Janusity is increased, at large enough values of ξ, the neck of the invagination containing the dimer decreases, while the angle between the principal axes of the NPs increases. Endocytosis occurs when the neck size becomes very small. Fig. S1 shows a snapshots time series of a dimer, at $J = 0.7$ and $\xi = 3.94 k_B T/\text{nm}^2$, undergoing endocytosis.

Although the equilibrium state of the system can be determined from direct molecular dynamics simulations at low values of J, the relative stability of the monomeric and dimeric states at moderate and high values of J, requires calculation of the free energies of the two states. This is achieved through WHAM using the distance d between the center beads of the NPs as the reaction coordinate. The free energies, for different values of the Janusity, in the case of $(D_{np}, \xi) = (10\text{ nm}, 4.33 k_B T/\text{nm}^2)$ and $(D_{np}, \xi) = (20\text{ nm}, 1.57 k_B T/\text{nm}^2)$ are shown in Figs. 6 and 8, respectively.

Fig. 6 shows that in the case of $D_{np} = 10$ nm and for $J \leq 0.2$, the free energy is practically independent of d, except for large values of d (i.e. for values of $d \gtrsim D_{ves} + D_{np} \approx 80$ nm). In this case, the NPs degree of wrapping is weak, as demonstrated by Fig. 3, and the vesicle shape is almost spherical, except for high values of d ($d \gtrsim 80$ nm) at which the adhering NPs elongate the vesicle along the axis connecting the two NPs centers, as shown by configuration (f) in Fig. 6 for $J = 0.2$ at $d = 90$ nm.

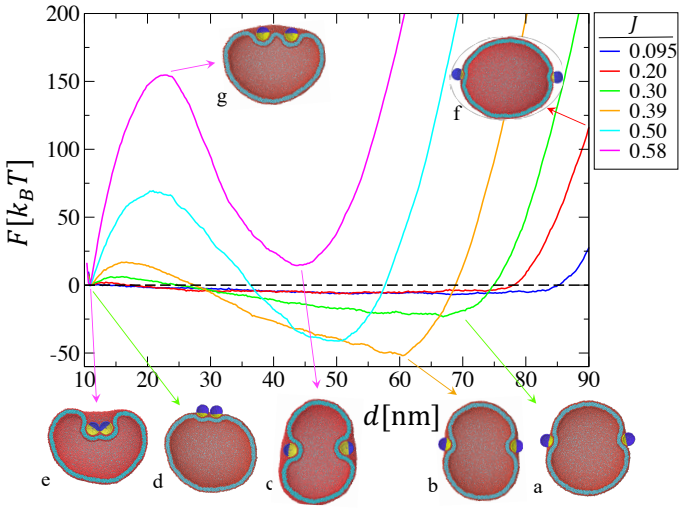

FIG. 6: Free energy, as obtained from WHAM, versus distance between two Janus 10-nm NPs, adhering to the outer side of the vesicle, for different values of J at $\xi = 4.33 k_B T/\text{nm}^2$. Snapshots (a), (b) and (c) correspond to the monomeric state at $J = 0.30$, 0.39 and 0.58, respectively. Snapshots (d) and (s) correspond to the monomeric state at $J = 0.30$ and 0.58, respectively. Snapshot (f) corresponds to an unstable state in which the vesicle is elongated at $J = 0.2$ at $d = 90$ nm. Snapshot (g) corresponds to an unstable state at the local maximum of the free energy at $J = 0.58$.

Fig. 6 shows that for $J \gtrsim 0.3$, the free energy exhibits two clear local minima. The first minimum occurs at $d_1 \approx D_{np} + 1$ nm and corresponds to the dimeric state. The second minimum occurs at a larger distance d_2 and corresponds to the monomeric state. At $J = 0.30$, this energy barrier is only about $6 k_B T$ from the dimeric state. This explains why the two NPs fairly quickly move away from each other when the initial distance between them is small at $J = 0.30$, as shown by the orange and cyan curves in Fig. 4 (A). In contrast, the relatively high energy barrier ($\approx 28 k_B T$) from the monomeric state at $J = 0.30$ prevents the two NPs, if initially far from each other, from sampling states in which they are dimerized, as shown by the red and blue curves Fig. 4 (A). However, at $J = 0.58$, the energy barrier from either the monomeric or dimeric state is much higher than $k_B T$. This explains why the NPs remain either in the monomeric or dimeric state at high J as shown by Fig. 4 (B). Fig. 6 shows that d_2 decreases with increasing J, which is associated with the increased flattening of the vesicle with J, along the plane perpendicular to the axis passing by the NPs centers. This flattening is due to the increased degree of wrapping of the NPs, as demonstrated by snapshots (a to c) in Fig. 6. The monomeric state is more stable than the dimeric state for $J \lesssim 0.5$, with an energy barrier that increases with increasing J. Fig. 6 shows that the dimeric state is more stable than the monomeric state at $J = 0.58$, which means that the

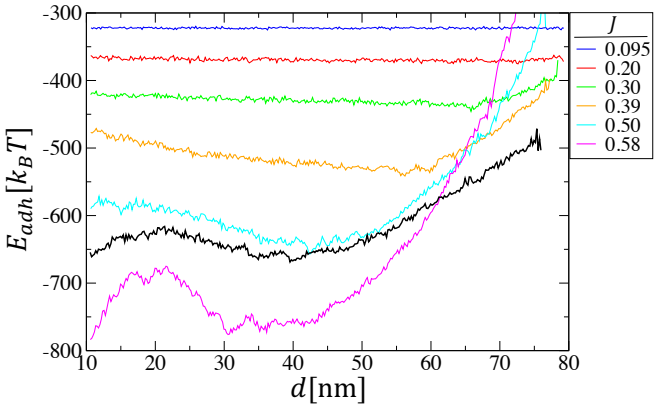

FIG. 7: Net adhesion energy of two 10-nm Janus NPs, adhering to the outer side of the vesicle at $\xi = 4.33k_BT/\text{nm}^2$, as a function of the distance between them. Curves for $J = 0.20$, 0.30, 0.39, 0.50, and 0.58 were translated upward by 350, 600, 950, 1350, and $1550k_BT$, respectively. The black curve corresponds to the case of $\xi = 6.0k_BT/\text{nm}^2$ at $J = 0.50$. This curve is translated upward by $2150k_BT$.

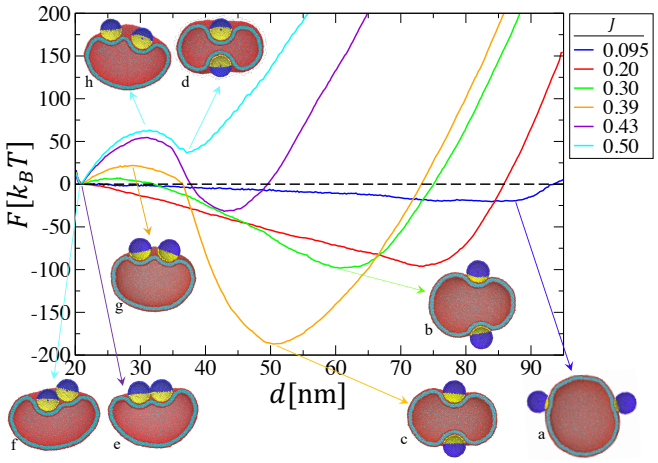

FIG. 8: Free energy versus distance between two Janus 20-nm NPs, adhering to the outer side of the vesicle, for different values of J in the case of $D_{np} = 20$ nm and $\xi = 1.57k_BT/\text{nm}^2$. Snapshots (a), (b), (c), and (d) correspond to the monomeric state at $J = 0.095$, 0.30, 0.39, and 0.50, respectively. Snapshots (e) and (f) correspond to the dimeric state at $J = 0.43$ and 0.50, respectively. (g) and (h) correspond to snapshots of the unstable state at the local maximum of the free energy tat $J = 0.39$ and 0.50, respectively.

transition from the monomeric to the dimeric state occurs at a value of J somewhere between 0.5 and 0.58. The fact that the energy barrier is much larger than k_BT for $J \gtrsim 0.4$ (*e.g.*, at $J = 0.5$, the energy barrier from the monomeric state to the dimeric state is about 3.5κ, and that from the dimeric to the monomeric state is about 2.3κ) implies that the final state of the system depends strongly on the initial placement of the NPs, rather than on the relative stability of the monomeric and dimeric states, in agreement with the results shown earlier in Fig. 4 for $J = 0.58$. For $J \gtrsim 0.65$, the monomeric state is locally stable, i.e., if the NPs initially adhere to the membrane at a distance larger than about 20 nm, they remain adhered in the monomeric state with typical configurations similar to that shown in Fig. 5. However, if the NPs adhere to the vesicle at a distance shorter than about 20 nm, they form a dimer, which is then endocytosed.

The results shown above are in good qualitative agreement with those by Bahrami and Weikl [31]. A difference between the present results and theirs, however, is that the dimeric state in their calculations becomes metastable only for $J \gtrsim 0.5$, whereas, in the present study, the dimeric state becomes metastable for $J \gtrsim 0.3$. Furthermore, they reported that due to their choice of a relatively high adhesion energy per unit of area ($\xi = 20\kappa/D_{np}^2$), the net adhesion energy of the NPs on the vesicle is independent of the distance between them. As a result the minimization of the energy amounts to the minimization of the curvature energy of the vesicle. In the present study, however, the net adhesion energy of the NPs varies with the distance between them, as demonstrated by Fig. 7 for the case of $D_{np} = 10$ nm. This dependence is particularly significant for $J \gtrsim 0.4$. These simulations correspond to the case where $\xi = 4.33k_BT \approx 14\kappa/D_{np}^2$, which although lower than that used in Ref. [31], it is in the regime where the degree of wrapping is practically in the saturation regime, as shown by Fig. 3(A).

To verify that the adhesion energy depends on d even at higher values of the adhesion energy density, simulations were performed at a value of the adhesion energy density equal to that in Ref. [31], i.e. at $\xi = 6k_BT/\text{nm}^2 = 20\kappa/D_{np}^2$. Here as well, the net adhesion energy is found to depend on the distance between the NPs, as shown by the black curve in Fig. 7. The discrepancy between the present results and those in Ref. [31] could be due to differences between the two models. The relatively large mesh size of the membrane, in Ref. [31], compared to the NPs diameter coupled to the fact that the interaction between the membrane vertices and an NP's surface is a square potential may result in inaccurate values of the adhesion energy. Therefore the equilibrium state of the system is not merely due to the minimization of the bending free energy. Moroever, the observed structures exhibit a high degree of fluctuations, which are neglected in Ref. [31]. Furthermore, since topological transformations of the vesicle are not allowed in Ref. [31], endocytosis of the NPs cannot occur. For example, it is highly plausible that the NPs dimer in Ref. [31] at $J = 0.7$ would be endocytosed.

The free energy versus d for the case of 20-nm NPs, shown in Fig. 8, has the same qualitative characteristics as those for the case of 10-nm NPs (Fig. 6). Namely, the dimeric state emerges at $J \gtrsim 0.2$, but remains less stable than the monomeric state for $J \lesssim 0.45$. However, the

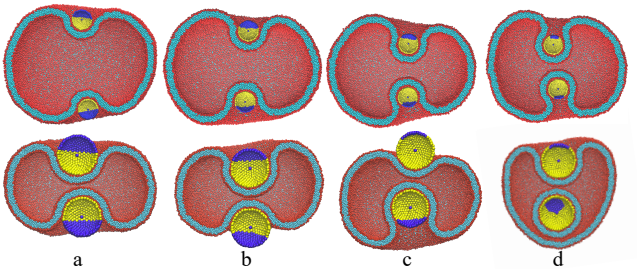

FIG. 9: Typical configurations of two Janus NPs, adhering to the outer side of a vesicle, in the monomeric state at high values of ξ. The top row corresponds to $D_{np} = 10$ nm at $\xi = 4.33 k_B T/\text{nm}^2$ and the bottom row corresponds to $D_{np} = 20$ nm at $\xi = 1.57 k_B T/\text{nm}^2$. (a), (b), (c), and (d) columns correspond to $J = 0.58$, 0.70, 0.80, and 0.90, respectively.

dimeric state becomes more stable than the monomeric state at higher values of J. The value of J at which the dimeric state becomes more stable than the monomeric state is lower in the case of 20-nm NPs than in the case of 10-nm NPs for same vesicle size. This implies that the vesicle-mediated attraction between the Janus NPs increases with increasing D_{np}/D_{ves}, in good agreement with Bahrami and Weikl's results [31]. It is interesting to note than in the case of 20-nm NPs at $J = 0.5$, the two NPs are not symmetrically positioned on the vesicle (see configuration (f) in Fig. 8). Namely, only one NP is well wrapped by the vesicle. The free energy of the dimeric state is lower than that of the monomeric state, at which both NPs are well wrapped (configuration (d) in Fig. 8), by $36 k_B T$. However, the adhesion energy of the dimeric state in the case of 20-nm NPs is $-2440 k_B T$, whereas that of the monomeric state is $-2660 k_B T$. The lower free energy of the dimeric state at $J = 0.5$ is therefore due to a lower contribution of curvature of the vesicle to the free energy in the dimeric state than in the monomeric state. This is qualitatively explained by the fact that the deformation of the vesicle in the dimeric state (snapshot (f) in Fig. 8) is less than that in the monomeric state (snapshot (d) in Fig. 8), since only one NP is significantly wrapped by the vesicle in the dimeric state.

Although the dimeric state is unstable against endocytosis at high values of J ($J \gtrsim 0.65$ for $D_{np} = 10$ nm and $J \gtrsim 0.55$ for $D_{np} = 20$ nm), the monomeric state is locally stable, due to the high energy barrier needed for the NPs to dimerize before they are endocytosed. The NPs in the monomeric state for the 10-nm NPs assume symmetric positions for all values of J, as shown by the top row of snapshots in Fig. 9 at $4.33 k_B T/\text{nm}^2$. However, for high values of D_{np}/D_{ves}, as in the case of 20-nm NPs, the NPs positions on the vesicle in the monomeric state and for $J \gtrsim 0.6$ are not symmetric, as demonstrated by Fig. 9. This is due to the fact that for high values of J, there is not enough material to wrap each NP by an area fraction equal to J. Interestingly, although endocytosis of single 10-nm NPs is not observed even for $J = 0.9$, Fig. 9 shows that one of the two 20-nm NPs is endocytosed. This allows the second NP to be more wrapped by the vesicle (see snapshot (d) versus (c) for $D_{np} = 20$ nm in Fig. 9).

B. Adhesion of Two Janus NPs on the Inner Leaflet of a Vesicle

We now turn to the situation where the Janus NPs adhere to the inner side of the vesicle. The corresponding free energy, extracted from WHAM, for the case of $D_{np} = 10$ nm is shown in Fig. 10 for different values of J. The free energy for the case of $D_{np} = 20$ nm is shown in Fig. S1 in Electronic Supplementary Information (ESI). Regardless of the value of J, Fig. 10 shows that the free energy, in the case where the NPs adhere to the inner side of the vesicle, exhibits a single minimum corresponding to the state where the NPs are apart from each other (i.e. monomeric state). The dimeric state, however, is unstable, which is contrasted with the case where the NPs adhere to the outer side of the vesicle, in which the dimeric state is either metastable or stable over a range of value of J. Furthermore, both Figs. 10 and S1 show that regardless of the size of the NPs, the preferred distance between them increases with J. This is also contrasted with the trend of the distance between NPs with J, in the case where they adhere to the outer side of the vesicle. These results are also in agreement with those of Bahrami and Weikl [31]. A difference between our results and theirs, however, is that their free energies are fairly flat over a wide range of distances, even for J as high as 0.7. Therefore, according to Ref. [31], the distance between the NPs must fluctuate over a wide range of values if they adhere to the inner side of the vesicle. This is not found to be the case, as demonstrated by Fig. 10, where the free energy versus d is relatively flat only for small values of J ($J \lesssim 0.3$). At intermediate and high values of J, however, the NPs remain fairly localized on the vesicle.

As in the case where the NPs adhere to the outer side of the vesicle, the net adhesion energy of the NPs, adhering to the inner side of the vesicle, also depends on the distance between the NPs, as shown by Fig. S2 in ESI for the case of 20-nm NPs. This implies that both the vesicle's curvature energy and the NPs' adhesion energy contribute to the free energy of the system.

IV. CONCLUSION

This article presents the results of a systematic investigation, based on molecular dynamics simulations of an implicit solvent model, of the modes of adhesion of two spherical Janus NPs on the inner or outer side of lipid vesicles. In this study, a Janus NP is constructed as tessellated shells, in which the vertices are connected with each other via harmonic springs and three-body inter-

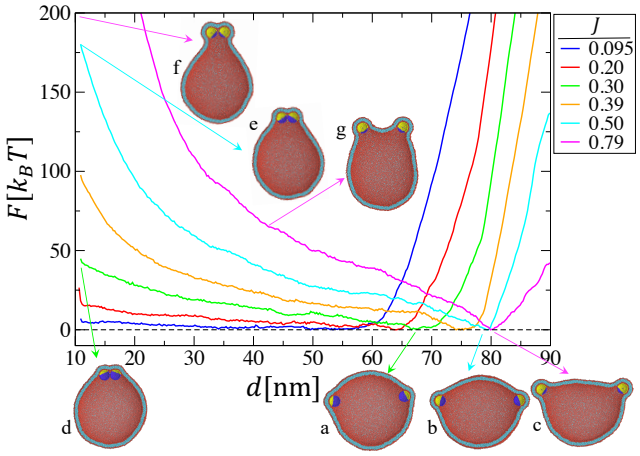

FIG. 10: Free energy versus distance between two 10-nm NPs, adhering to the inner side the vesicle, for different values of J at $\xi = 4.33 k_B T/\text{nm}^2$. Snapshots (a), (b), and (c) correspond to most stable states at $J = 0.30$, 0.50, and 0.79, respectively. Snapshots (d), (e), and (f) correspond to the dimeric state ($d = 11$ nm) for $J = 0.30$, 0.50 , and 0.79, respectively. Snapshot (g) is for $J = 0.79$ at $d = 40$ nm.

actions. The rigidity of the NP is further enhanced by the addition of a bead at the center of the NP, which is connected to all vertices by fairly rigid harmonic springs. The preferred placement of the NPs outside or inside the vesicle is determined from free energy calculations using the weighted histogram analysis method [37].

The free energy calculations show that the NPs exhibit two modes of adhesion in the case where they adhere to the outer side of the vesicle. The first one, which corresponds to the monomeric state, occurs at relatively low values of the area fraction, J, of the NPs that interact attractively with the lipids head groups. For intermediate values of J, the NPs prefer to dimerize into an in plane dimer. The energy barrier between the monomeric and dimeric states is much higher than k_BT at intermediate values of J. This implies that the final placement of the NPs on the vesicle depends on their initial position upon their adhesion. Therefore, the NPs are dimerized if their initial positions on the vesicle are close to each other. However, the NPs remain apart from each other if their initial positions are far from each other. In contrast to the case where the NPs adhere to the outer side of the vesicle, the dimeric state of Janus NPs adhering to the inner side of vesicles is found to be unstable, regardless of J and the ratio between the diameters of the NPs and vesicle. In the limit of vesicles with infinite radius, i.e. in the case of planar membranes, the distinction between the cases where the NPs adhering to the outer or inner side of the vesicle disappears. Therefore, one expects that the energy barrier between the dimeric and monomeric states, in the case where the NPs adhere to the outer side of the vesicle, to decrease with increasing the vesicle's size. Indeed, we performed simulations of two Janus NPs at $\xi = 1.57 k_B T/\text{nm}^2$ on a tensionless planar bilayer in the case of $J = 0.5$ and found that the dimeric state is unstable.

The results presented in this article are largely in agreement with those presented earlier by Bahrami and Wiekl [31]. However, the following differences are noted. In their approach, which is based on an energy minimization of dynamically triangulated vesicles and therefore neglects the effect of thermal fluctuations, the adhesion energy of the NPs is found to be independent of the distance between them. Therefore, the equilibrium state is found from the minimization of the vesicles curvature energy, which in their model is described by the Helfrich Hamiltonian [46]. In contrast, however, we found that the adhesion energy of the NPs depends on the distance between them, with this dependence becoming increasingly important as J is increased. Therefore the adhesion energy plays a role on the equilibrium state of the system. Furthermore, the vesicle's topology is conserved in their approach. As a result they found that the dimeric state of the NPs, that adhere to the outer side of the vesicle, occurs at values of J at which we observe endocytosis of the dimerized NPs.

Much of the interest on Janus NPs is driven by their ability to self-assemble into interesting superstructures [47]. These NPs are typically hydrophilic, i.e. with one moiety that is anchored with a hydrophilic ligand and the other moiety that is anchored with a hydrophobic ligand. Both moieties of the Janus NPs considered in the present study, however, have to be hydrophilic to allow them to interact attractively both with the lipid head groups and the aqueous solvent, while interacting repulsively with the hydrophobic lipid tail groups. Such Janus NPs can, for example, be synthesized such that one moiety is capped with citrate and the other moiety is decorated with short poly-ethylene glycol chains.

Conflicts of Interest

There are no conflicts to declare.

Acknowledgements

This work was supported by a grant from the National Science Foundation (DMR-1931837). All simulations were performed on computers of the High Performance Computing Facility at the University of Memphis. All snapshots in this article were generated using VMD version 1.9.3 [48].

[1] M. Wang, A. M. Mihut, E. Rieloff, A. P. Dabkowska, L. K. Møansson, J. N. Immink, E. Sparr, and J. J. Crassous, *Proc. Nat. Acad. Sci.*, 2019, **116**, 5442-5450.
[2] R. Lipowsky and H. -G. Döbereiner, *Europhys. Lett.*, 1998, **43**, 219–225.
[3] M. Deserno and W. M. Gelbart, *J. Phys. Chem. B*, 2002, **106**, 5543-5552.
[4] M. Deserno and T. Bickel, *Europhys. Lett.*, 2003, **62**, 767-773.
[5] E. J. Spangler, S. Upreti, and M. Laradji, *J. Chem. Phys.*, 2016, **144**, 044901.
[6] I. Koltover, J. O. Rädler, and C. R. Safinya, *Phys. Rev. Lett.*, 1999, **82**, 1991-1994.
[7] L. Ramos, T. Lubensky, N. Dan, P. Nelson, and D. Weitz, *Science*, 1999, **286**, 2325-2328.
[8] A. Xi and G. Bothun, *Analyst*, 2014, **139**, 973-981.
[9] K. Sugikawa, T. Kadota, K. Yasuhara, and A. Ikeda, *Angew. Chem. Int. Ed.*, 2016, **55**, 4059-4063.
[10] C. van der Wel, A. Vahid, A. Saric, T. Idema, D. Heinrich, and D. J. Kraft, *Scientific Rep.*, 2016, **6**, 32825.
[11] A. Šarić and A. Cacciuto, *Phys. Rev. Lett.*, 2012, **109**, 188101.
[12] A. Šarić and A. Cacciuto, *Phys. Rev. Lett.*, 2012, **108**, 188101.
[13] A. H. Bahrami, R. Lipowsky, and T. R. Weikl, *Phys. Rev. Lett.*. 2012, **109**, 188102.
[14] A. D. Olinger, E. J. Spangler, P. B. Sunil Kumar, and M. Laradji, *Faraday Disc.*, 2016, **186**, 265-275.
[15] E. J. Spangler, P. B. S. Kumar, and M. Laradji, *Soft Matter*, 2018, **14**, 5019–5030.
[16] E. J. Spangler and M. Laradji, *J. Chem. Phys.*, 2021, **154**, 244902.
[17] K. Xiong, J. Zhao, D. Yang, Q. Cheng, J. Wang, and H. Ji, *Soft Matter*, 2017, **13**, 4644–4652.
[18] B. J. Reynwar, G. Illya, V. A. Harmandaris, M. M. Müller, K. Kremer, and M. Deserno, *Nature* , 2007, **447**, 461-464.
[19] S. E. A. Gratton, P. A. Ropp, P. D. Pohlhaus, J. C. Luft, V. J. Madden, M. E. Napier, and J. M. DeSimone, *Proc. Natl. Acad. Sci. U. S. A.*, 2008, **105**, 11613-11618.
[20] X. Yi, X. Shi, and H. Gao, *Nano Lett.*, 2014, **14**, 1049-1055.
[21] S. Dasgupta, T. Auth, and G. Gompper, *Nano Lett.*, 2014, **14**, 687-693.
[22] Y. Yin, A. Arkhipov, and K. Schulten, *Structure*, 2009, **17**, 882-892.
[23] H. Yu and K. Schulten, *PLoS Comput. Biol.*, 2013, **9**, e1002892.
[24] M. Simunovic, A. Šarić, J. M. Henderson, K. Y. C. Lee, and G. A. Voth, *ACS Cent. Sci.*, 2017, **3**, 1246–1253.
[25] F. Bonazzi and T.R. Weikl, *Biophys. J.*, 2019, **116**, 1239-1247.
[26] E. J. Spangler, A. D. Olinger, P. B. Sunil Kumar, and M. Laradji, *Soft Matter*, 2021, **17**, 1016-1027.
[27] C. Kaewsaneha, P. Tangboriboonrat, D. Polpanich, M. Eissa, and A. Elaissari, *ACS Appl. Mater. Interfaces*, 2013, **5**, 1857-1869.
[28] D. Wu and A. Honciuc, *ACS Appl. Nano Mater.*, 2018, **1**, 471-482.
[29] B. G. Cha, Y. Piao, and J. Kim, *Mater. Res. Bull.*, 2015, **70**, 424-429.
[30] X. Zhang, Q. Fu, H. Duan, J. Song, and H. Yang, *ACS Nano*, 2021, **15**, 6147–6191.
[31] A. H. Bahrami and T. R. Weikl, *Nano Lett.*, 2018, **18**, 1259–1263.
[32] J. T. Wiemann, Z. Shen, H. Ye, Y. Li, and Y. Yu, *Nanoscale*, 2020, **12**, 20326-20336.
[33] L. Ou, C. Corradi, D. P. Tieleman, and Q. Liang, *J. Phys. Chem. B*, 2020, **124**, 4466-4475.
[34] A. Alexeev, W. E. Uspal, and A. C. Balazs, *ACS Nano*, 2008, **2**, 1117-1122.
[35] K. Lee, L. Zhang, Y. Yi, X. Wang, and Y. Yu, *ACS Nano*, 2018, **12**, 3646-3657.
[36] J. R. Baumgardner and P. O. Frederickson, *SIAM J. Numer. Anal.*, 1985, **22**, 1107–1115.
[37] S. Kumar, D. Bouzida, R. H. Swendsen, P. A. Kollman, and J. M. Rosenberg, *J. Comput. Chem.*, 1992, **13**, 1011–1021.
[38] J. D. Revalee, M. Laradji, and P. B. Sunil Kumar, *J. Chem. Phys.*, 2008, **28**, 035102.
[39] M. Laradji, P. B. Sunil Kumar, and E. J. Spangler, *J. Phys. D.: Appl. Phys.*, 2016, **49**, 293001.
[40] G. S. Grest and K. Kremer, *Phys. Rev. A* , 1986, **33**, 3628–3631.
[41] W. C. Swope, H. C. Andersen, P. H. Berens, and K. R. Wilson, *J. Chem. Phys.*, 1982, **76**, 637–649.
[42] J. F. Nagle, M. S. Jablin, S. Tristram-Nagle, and K. Akabori, *Chem. Phys. Lipids*, 2015, **185**, 3–10.
[43] G. M. Torrie and J. P. Valleau, *Chem. Phys. Lett.*, 1974, **28**, 578-581.
[44] K. A. Smith, D. Jasnow, and A. C. Balazs, *J. Chem. Phys.*, 2007, **127**, 084703.
[45] M. Laradji, P. B. Sunil Kumar, and E. J. Spangler, *Chem. Phys. Lipids*, 2020, **233**, 104989.
[46] W. Helfrich, *Z. Naturforsch.*, 1973, **28c**, 693-703.
[47] C. Kang and A. Honciuc, *J. Phys. Chem. Lett.*, 2018, **9**, 1415-1421.
[48] W. Humphrey, A. Dalke, and K. Schulten, *J. Mol. Graphics*, 1996, **14**, 33-38.